JOC The Journal of Organic Chemistry

Featured Article

pubs.acs.org/joc

Solvent-Dependent Decarboxylation of 1,3-Dimethylimdazolium-2-Carboxylate

Derek M. Denning and Daniel E. Falvey*

Department of Chemistry and Biochemistry, University of Maryland, College Park, Maryland 20742, United States

Supporting Information

ABSTRACT: 1,3-Dimethylimidazolium-2-carboxylate **1** is stable in both pure water and pure acetonitrile. However, in mixtures of the two solvents, this compound suffers a rapid decarboxylation/protonaton reaction, forming 1,3-dimethylimidazolium cation **2**. A series of kinetic and mechanistic experiments, along with DFT calculations, were carried out to understand the mechanism of this process and to elucidate the role of solvation on the stability of **1**. These findings demonstrate that the decomposition process is a reversible decarboxylation forming the corresponding *N*-heterocyclic carbene (1,3-dimethylimidazolylidene, **3**), followed by a rapid protonation of **3** by water or other protic species. The length and strength of the C−C bond between in the imidazolium ring and the carboxylate group (denoted $C_{NHC}-CO_2$) of **1** is remarkably dependent on the polarity of the solvent. Density functional theory (DFT) calculations predict a ca. 20 kcal/mol change in the barrier to decarboxylation in going from the gas phase to (SMD-simulated) water. Thus, addition of water has two effects on the stability of **1**. At low concentrations, it provides a proton source for the trapping of the carbene **3** and accelerates decomposition. At higher concentrations, it increases the polarity of the medium. slowing the decarboxylation process and likewise the overall decomposition rate.

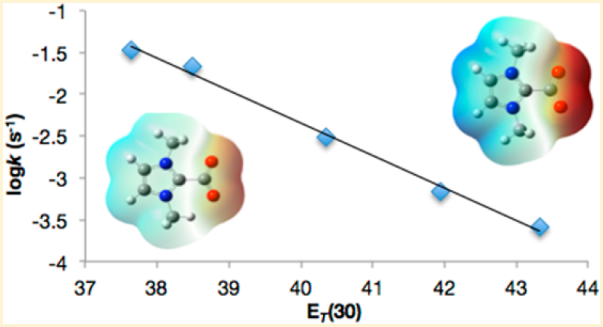

INTRODUCTION

Concern over the impact of carbon dioxide and its role in climate change has motivated efforts to search for new ways to mitigate the release of this greenhouse gas into the atmosphere. One strategy known as carbon capture and storage (CCS)[1,2] entails developing materials or reagents that can reversibly bind to CO_2, either for long-term storage or in conjunction with chemical reagents that could render CO_2 into useful chemicals and/or fuels.[3] A variety of materials including metal organic frameworks,[4] polyamine adsorbent materials,[5,6] frustrated Lewis pairs,[7−9] and ionic liquids[10] have been examined as possible CCS reagents. The current study focuses on *N*-heterocyclic carbenes (NHCs) and their addition to CO_2 to yield stable zwitterionic imidazolium-2-carboxylates ($NHC-CO_2$) (Figure 1).

The first report of the isolation of these species came when Kuhn and co-workers reported the addition of 1,3-diisopropyl-4,5-dimethylimidazolylidene to carbon dioxide to give an air-stable $NHC-CO_2$.[11] Since then, these species have seen use as precursors for NHCs, as organocatalysts for carbonate synthesis,[12,13] and as agents for ligand transfer to transition metals.[14−16] $NHC-CO_2$ have also been used as CO_2-transfer reagents,[17−20] and some mechanistic studies have been carried out on them.[21,22] Additionally, computational work has shown that substituent effects on the imidazolium ring can dramatically impact the binding energy to CO_2 in the gas phase.[23] Imidazolium-2-carboxylates are generally poorly soluble in organic solvents such as THF, MeCN, and CH_2Cl_2 unless tetraphenylborate salts are added.[24] In contrast, 1,3-dimethylimidazolium-2-carboxylate **1** exhibits good solubility in H_2O.

While it is clear that NHC carboxylation is a reversible process, there is some ambiguity regarding the stability of these adducts under various conditions. For example, Taton et al. report rapid conversion of $NHC-CO_2$ species to the corresponding imidazolium cation and hydrogen carbonate in organic solvents upon addition of water.[21] On the other hand, Crabtree et al. report NMR characterization of these species in aqueous solution.[15] In the course of some photochemical studies (which will be reported elsewhere), we likewise found that $NHC-CO_2$ was stable in rigorously anhydrous CH_3CN as well as in neat H_2O but that it decomposed rapidly in mixed CH_3CN/H_2O solvent systems. In order to understand this apparently anomalous solvent dependence we undertook a series of

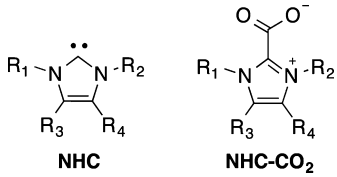

Figure 1. Structures of *N*-heterocyclic carbenes (NHC) and imidazolium 2-carboxylates ($NHC-CO_2$).

Received: April 2, 2014
Published: April 24, 2014

   dx.doi.org/10.1021/jo5007575 | J. Org. Chem. 2014, 79, 4293−4299

experimental and computational studies on the decomposition process of **1** (Scheme 1). The findings, described below, show

Scheme 1. Concerted and Stepwise Possible Mechanisms for the Decomposition of 1 in Binary Solvent Mixtures

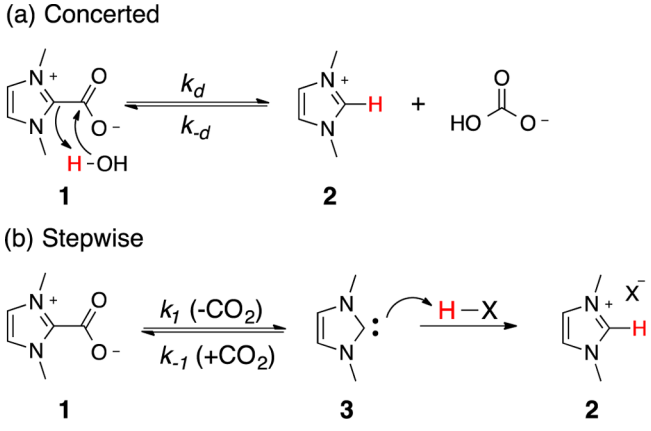

that the rate of decarboxylation of **1** is strongly dependent on the polarity of the medium, being rapid in nonpolar solvents and slow in more polar media. However, in the absence of a strong proton donor, this decarboxylation process is reversible and, to the extent protic species are excluded, leads to no net conversion of starting materials. Computational studies at the DFT level using the SMD implicit solvation model attribute this stability to the degree of zwitterionic character. Polar solvents favor a shorter stronger C_{NHC}−CO_2 and a higher degree of charge separation between the imidazolium and carboxylate. In the gas phase and nonpolar solvents this bond lengthens and weakens accompanied by reduced charge separation.

RESULTS AND DISCUSSION

1,3-Dimethylimidazolium-carboxylate **1** was prepared by heating a mixture of 1-methylimidazole and dimethyl carbonate in a sealed tube as described previously.[25] In D_2O this material shows ^1H and ^{13}C NMR spectra consistent with previous reports. Despite limited solubility it was also possible to characterize the ^1H NMR spectrum of this species in CD_3CN. In this solvent, **1** appears to be indefinitely stable, showing only minor (see the Supporting Information) decomposition over 58 h. However, when a small drop of D_2O is added to the CD_3CN solution, the signals for **1** are rapidly and cleanly replaced by those for the 1,3-dimethylimidazolium cation **2**, while no other significant products could be detected in the ^1H NMR spectrum.

This decomposition reaction could also be monitored by UV−vis spectroscopy. Under the solvent conditions below, carboxylate **1** shows a λ_{max} ca. 227 nm and the product, imidazolium cation has a λ_{max} ca. 211 nm. As shown in (Figure 2, top) the reactant, **1** converts cleanly to the product **2** with an isosbestic point near 211 nm. The decay, followed at 240 nm, fits to an apparent first order rate law in several cases that we examined in detail (Figure 2, bottom). For the purposes of comparing rate behavior, however, the rate constants in Tables 1−3 and 7 were determined by the initial rate method.

The rate of decomposition of **1** was monitored in various mixtures of water and an organic solvent (1,4-dioxane, acetonitrile, methanol). The data, listed in Table 1, show a correlation between the amount of water and the rate constant for decomposition. Increasing water reduces the rate of

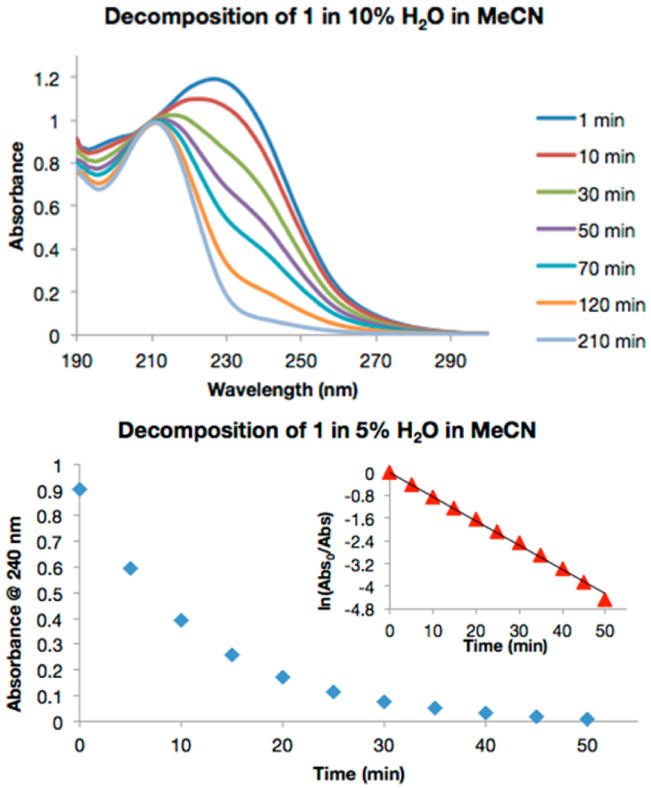

Figure 2. UV−vis absorption spectrum at varying times following addition of **1** to CH_3CN with 10% H_2O (top). Time-dependent decomposition of **1** in 5% H_2O in MeCN monitored at 240 nm with first-order rate plot (bottom).

decomposition in each solvent examined. As illustrated in Figure 3, the rate constants in 1,4-dioxane/H_2O mixtures are dramatically reduced over the range of 0−10% H_2O and then show smaller variation at higher concentrations. Likewise, at a given water concentration, the rate constant for decomposition depends on the polarity of the solvent, being slowest in the most polar solvent studied, CH_3OH, and fastest in the least polar solvent, 1,4-dioxane, with CH_3CN providing intermediate values.

While the data noted above establish a robust trend for increasing stability with increasing solvent polarity, the stability of **1** in pure organic solvents, such as CH_3CN is less clear. Given that the product includes a proton in addition to the loss of carbon dioxide, one plausible mechanism would be a concerted protonation/decarboxylation (Scheme 1a). In that case the decomposition rate would be dependent on the concentration and strength of the proton donor. A stepwise mechanism involving irreversible decarboxylation followed by protonation (Scheme 1b, where k_{-1} is negligible) would be expected to show decomposition rates that are independent of the concentration or strength of the proton source. In that case, decomposition in pure acetonitrile would be faster (due to the lower polarity) than what is observed in CH_3CN/H_2O mixtures. Finally, a reversible stepwise mechanism would show dependence on water (or more generally any proton donor) at low concentrations. However, at high concentrations of water, decarboxylation would become rate limiting, and the effect of additional water would be to alter the polarity of the medium.

The following experiments cause us to favor the latter, stepwise reversible mechanism.

dx.doi.org/10.1021/jo5007575 | J. Org. Chem. 2014, 79, 4293−4299

Table 1. Decomposition Rate Constants (s^{-1}) for 1 in Various Solvent Mixtures

% H_2O	1,4-dioxane	acetonitrile	methanol
3.0	$(3.32 \pm 0.09) \times 10^{-2}$	$(3.67 \pm 0.83) \times 10^{-3}$	$(1.37 \pm 0.25) \times 10^{-4}$
5.0	$(2.18 \pm 0.12) \times 10^{-2}$	$(1.04 \pm 0.25) \times 10^{-3}$	$(8.84 \pm 0.45) \times 10^{-5}$
10.0	$(3.12 \pm 0.24) \times 10^{-3}$	$(2.48 \pm 0.30) \times 10^{-4}$	$(4.00 \pm 0.42) \times 10^{-5}$
15.0	$(6.83 \pm 0.13) \times 10^{-4}$	$(9.00 \pm 0.57) \times 10^{-5}$	$(1.33 \pm 0.72) \times 10^{-5}$
20.0	$(2.57 \pm 0.17) \times 10^{-4}$	$(4.43 \pm 0.31) \times 10^{-5}$	$(6.22 \pm 0.67) \times 10^{-6}$

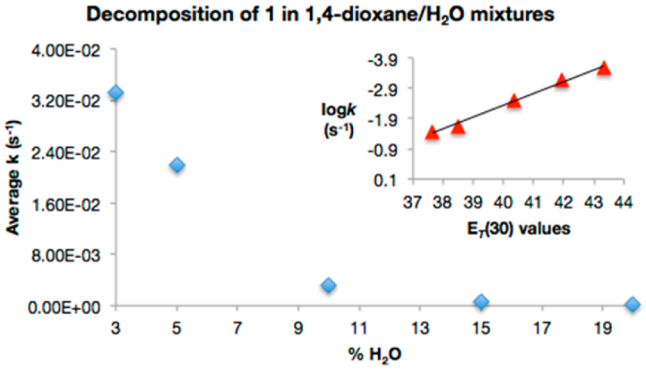

Figure 3. Average initial rate constants (s^{-1}) for the decomposition of **1** in 1,4-dioxane/H_2O mixtures measured at 240 nm.

(1) Exchange of labeled CO_2 into **1**. In this experiment, CD_3CN solutions of **1** were purged with natural abundance CO_2 or $^{13}CO_2$ for 20 min and then ^{13}C NMR spectra were acquired for both solutions. Both solutions show mostly recovered **1** accompanied by HCO_3 and some trace imidazolium ion. However, the solution treated with $^{13}CO_2$ shows a dramatic increase in the carboxylate ^{13}C resonance for **1** at 155.9 ppm (Figure 4), confirming that the labeled CO_2 exchanged with the unlabeled carboxyl group and would be consistent with either of the reversible mechanisms shown in Scheme 1. However, this exchange result combined with the slowing of the decomposition rate at high water concentrations causes us to favor the reversible, stepwise mechanism shown in Scheme 1b.

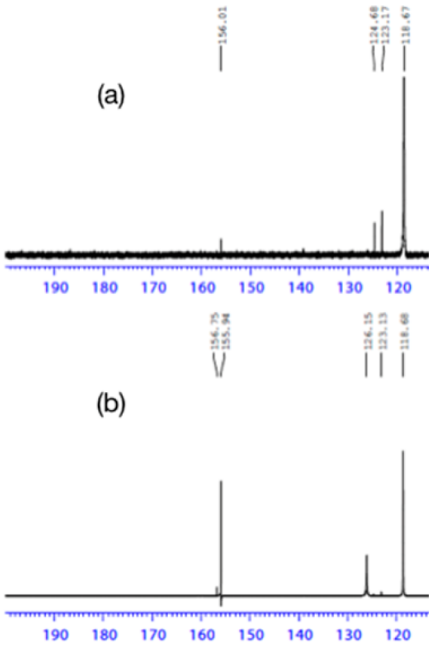

Figure 4. ^{13}C NMR spectra from **1** dissolved in CD_3CN after purging with (a) unlabeled CO_2 and (b) ^{13}C-labeled CO_2.

(2) Inhibition of decomposition by CO_2. Rate constants listed in Table 3 were obtained in solutions that were saturated with CO_2 and can be compared with those in Table 1. In each solvent and water concentrations of 5−10% examined there is a modest, but consistent, decrease in the overall rate constant as would be expected for the stepwise reversible process. Mechanisms involving concerted protonation/decarboxylation or irreversible decarboxylation would show no rate dependence on added CO_2.

(3) H/D kinetic isotope effects. An irreversible decarboxylation followed by rapid protonation would be expected to show identical decomposition rate constants in D_2O and H_2O. A concerted protonation/decarboxylation mechanism should show a primary kinetic isotope effect. The reversible, stepwise mechanism is expected to show a primary isotope effect at low water concentrations, where proton/deuterium transfer is rate limiting and then a transition to no isotope effect at high water concentrations, where decarboxylation is rate limiting. As shown in Table 2, k_H/k_D of 1.33 is observed in 5% H_2O/D_2O in dioxane, and this diminishes to 1.08 in 20% H_2O/D_2O.

Table 2. Decomposition Rate Constants (s^{-1}) for 1 in 1,4-Dioxane/D_2O Solvent Mixtures

% D_2O	1,4-dioxane	k_H/k_D
5.0	$(1.64 \pm 0.65) \times 10^{-2}$	1.33
10.0	$(2.41 \pm 0.05) \times 10^{-3}$	1.29
15.0	$(5.90 \pm 0.03) \times 10^{-4}$	1.16
20.0	$(2.37 \pm 0.04) \times 10^{-4}$	1.08

(4) Partial decay of **1** with trace amounts of H_2O. The results of these three experiments motivated a closer examination of the behavior of **1** in nominally anhydrous CH_3CN. Specifically, a dilute solution of **1** was prepared in CH_3CN that had been distilled from CaH_2, and the UV−vis absorption at 240 nm was monitored as a function of time. As shown in Figure 5, this signal shows an initial decay over a time period of ca. 4 h followed by a longer phase of up to 13 h, where there is negligible change in the signal. This behavior is consistent with decarboxylation followed by protonation by the residual water (CH_3CN is very difficult to completely dry). Once the water is consumed, the carbene **3** forms reversibly and there is no net change in composition. It is possible that **3** (conjugate acid pK_a ca. 23.0)[26] slowly deprotonates CH_3CN (pK_a = 25.0) In fact, Louie et al. have described such reactions from a related carbene.[24] Such processes would result in the decomposition of **1** over a much longer time scale than what was examined in the current study.

dx.doi.org/10.1021/jo5007575 | J. Org. Chem. 2014, 79, 4293−4299

Table 3. Decomposition Rate Constants (s^{-1}) for 1 in Various Solvent Mixtures Purged with CO_2

% H_2O	1,4-dioxane	acetonitrile	methanol
5.0	$(1.94 \pm 0.07) \times 10^{-2}$	$(8.14 \pm 0.23) \times 10^{-4}$	$(6.60 \pm 0.20) \times 10^{-5}$
10.0	$(2.05 \pm 0.15) \times 10^{-3}$	$(1.87 \pm 0.05) \times 10^{-4}$	$(3.03 \pm 0.38) \times 10^{-5}$
15.0	$(6.31 \pm 0.50) \times 10^{-4}$	$(8.16 \pm 0.51) \times 10^{-5}$	$(1.28 \pm 0.12) \times 10^{-5}$

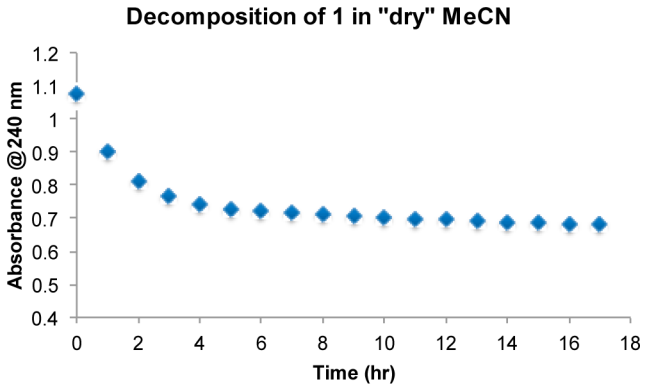

Figure 5. Time dependence of 240 nm absorption for **1** in nominally dry CH_3CN.

The reversible, stepwise mechanism supported by experiments 1−4 above accounts for the stability of **1** in aprotic media. However, it does not directly explain the stability of **1** in water, and more generally, in polar solvents. To this end, DFT calculations were used to characterize the structure of **1** and its transition state leading to decarboxylation. For gas-phase calculations, the structure of **1** was optimized at the B3LYP/6-31G(d,p) level[27,28] and stationary points were identified as local minima or transition states by analysis of the calculated vibrational frequencies. In general, these calculations provided three stationary points: minima corresponding to structure **1**, a weakly bound molecular complex consisting of carbene **3** and CO_2, as well as a transition state connecting these two minima. These are illustrated in Figure 6. Absent solvation, these calculations show an elongated $C_{NHC}-CO_2$ bond for **1** with a distance of 1.576 Å, which is ca. 3.8 kcal/mol below the complex. The corresponding transition state shows a low barrier of ca. 6.4 kcal/mol.

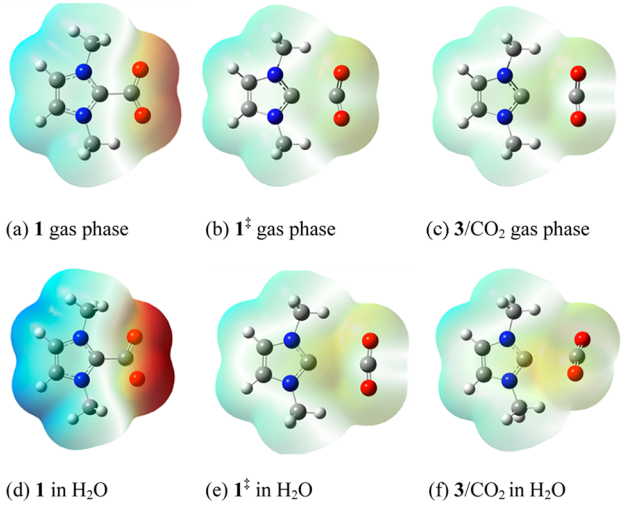

Figure 6. Structures derived from DFT optimizations on **1** (a, d), $\mathbf{1}^{\ddagger}$ (b,e), and **3**/CO_2 (c, f) in the gas phase (a−c) and water (d−f), as simulated using the SMD implicit solvation model. The shaded isosurfaces are representations of the molecular electrostatic potential, where dark blue denotes positive charge (+0.092) and dark red denotes negative charge (−0.092).

Because the solvent polarity has a significant effect on the stability of **1**, it was important to identify an experimental benchmark that could be used to validate possible theoretical treatments of solvation. Therefore, the Gibbs free energy barrier for decomposition ($\Delta G^{\ddagger}$) of **1** was experimentally characterized by fitting the temperature dependence of the decomposition rate k_d constants for **1** in water to the Eyring equation (1). For our purposes, the transmission coefficient, κ, was assumed to be 1.00; k_b, h, and R are, respectively, Boltzmann's constant, Planck's constant, and the gas constant. The results of this analysis, shown in Figure 7 provide an experimental value of $\Delta G^{\ddagger}$ = 24.9 kcal/mol. This barrier was then modeled by carrying out calculations on **1**, the **3**/CO_2 complex, and the corresponding transition state using various implicit solvation models. The results are summarized in Table 4.

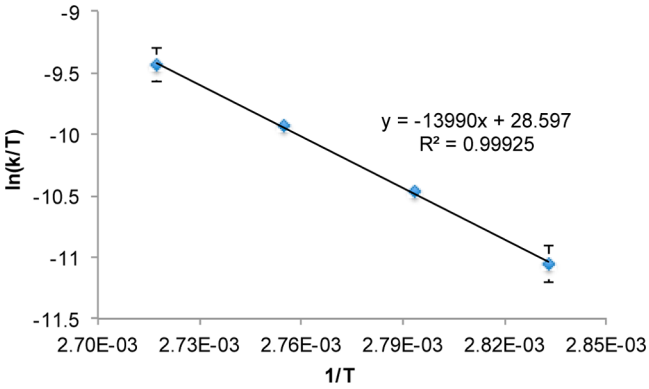

Figure 7. Eyring analysis of the temperature dependence (T, in K) for the decomposition rate constants for **1** (k, in s^{-1}) in H_2O.

$$k_d = \frac{\kappa k_b T}{h} \exp[\Delta G^{\ddagger}/RT] \quad (1)$$

The SMD implicit solvation model developed by Truhlar and Cramer[29] predicts 25.1 kcal/mol and shows excellent agreement with the experimental barrier. It was therefore used for the more

Table 4. Comparison of Computed Gibbs Free Energy Barriers for Decarboxylation of 1 Using Various Implicit Solvation Models and Experiment

model/expt	$\Delta G^{\ddagger}$ (kcal/mol)
SMD[a]	25.1
CPCM[b]	16.1
IEF-PCM[c]	16.0
PCM[d]	16.0
expt	24.9 ± 0.28

[a]Reference 29. [b]References 30 and 31. [c]Reference 32. [d]References 33 and 34.

dx.doi.org/10.1021/jo5007575 | J. Org. Chem. 2014, 79, 4293−4299

Table 5. Selected Geometric Parameters, Dipole Moments (D), and Free Energies, Computed for 1 and 1‡ Using the B3LYP/6-31G(d,p) and the SMD Implicit Solvation Model

solvent	$E_T(30)$ value	$C_{NHC}-CO_2$ (Å)	$CO_2 \angle$ (deg)	D	$\Delta G^{\ddagger}$ (kcal/mol)	$C_{NHC}-CO_2^{\ddagger}$ (Å)	ΔG^0 (kcal/mol)	$D^{\ddagger}$
Gas	27.1	1.576	133.7	9.13	6.37	2.310	3.83	5.14
1,4-dioxane	36.0	1.568	132.0	10.3	10.2	2.438	9.26	5.17
THF	37.4	1.554	132.0	11.2	14.7	2.495	13.0	5.40
CH_2Cl_2	40.7	1.555	130.7	11.6	15.3	2.519	13.9	5.33
MeCN	45.6	1.541	131.1	12.0	17.0	2.513	14.7	5.57
1-decanol	47.7	1.538	129.9	12.3	20.3	2.591	19.4	5.06
EtOH	51.9	1.528	129.5	13.0	22.0	2.551	21.0	5.54
MeOH	55.4	1.530	129.1	13.1	23.8	2.592	22.2	5.36
H_2O	63.1	1.522	128.8	13.4	25.1	2.792	24.4	4.59

detailed studies described below. Other implicit models faired far worse. For example, the IEF-PCM algorithm (the default model in the Gaussian09 package) differed by more than 10 kcal/mol from the experimental value.

Table 5 illustrates selected geometric parameters, dissociation free energies (ΔG^0 defined as the difference between **1** and the **3**/CO_2 complex), and activation free energies ($\Delta G^{\ddagger}$) predicted for **1** in various solvents calculated using B3LYP/6-31G(d,p)/SMD. As with the experimental data, there is a dramatic dependence on the solvent polarity. For example, the activation free energy increases by nearly 20 kcal/mol in going from the gas phase to water. In fact, Figure 8 shows a clear linear free energy

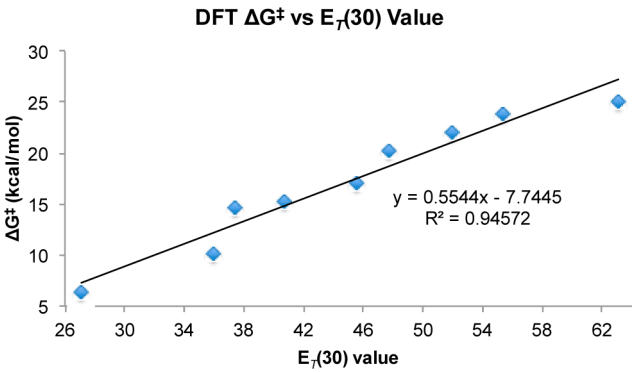

Figure 8. Linear free energy relationship between the calculated $\Delta G^{\ddagger}$ and Reichardt's $E_T(30)$ solvation parameter.

relationship between the calculated $\Delta G^{\ddagger}$ and Reichardt's $E_T(30)$ solvation parameter.[35,36] This weakening of the $C_{NHC}-CO_2$ bond is also reflected in the change in length of the corresponding bond distance, which diminishes from 1.576 Å in the gas phase to 1.522 Å in aqueous solution. Interestingly, the dipole moment of **1** is predicted to increase, despite the shorter bond distance. It is also notable that the transition state $C_{NHC}-CO_2$ bond distances ($\mathbf{C_{NHC}-CO_2^{\ddagger}}$) tend to increase with increasing solvent polarity. This trend reflects the product-like transition states associated with these increasingly endergonic reactions as would be expected on the basis of the Hammond postulate.

In considering the structure of **1**, it appears that $C_{NHC}-CO_2$ bond formation is accompanied by increasing charge transfer to the CO_2 group. The effect of increasing solvent polarity is to favor a shorter, stronger, and more polarized bond. Figure 6 illustrates this point through a visualization of ESP on the structure of **1** optimized in the gas phase and in aqueous solution. The latter shows a significantly increased accumulation of negative charge on the CO_2 group compared with the gas-phase structure. Also illustrated are ESP surfaces for the corresponding transition states. In both cases, scission of the $C_{NHC}-CO_2$ bond is accompanied by a diminishment of charge separation and thus should be favored in less polar solvents.

The explanation whereby of increasing carboxyl group charge leading to a stronger $C_{NHC}-CO_2$ bond lead us to examine other methods for strengthening this bond. Specifically, it was reasoned that binding a Lewis acid, in the form of a cation, to the carboxylate group would have an effect of stabilizing **1** relative to decarboxylation and protonation. This prediction was tested both computationally and experimentally. Table 6 compares the

Table 6. Selected Geometric Parameters Computed for 1 with Cations Using B3LYP/6-31G(d,p) and the SMD Implicit Solvation Model

cation	$C_{NHC}-CO_2$ (Å)	$CO_2 \angle$ (deg)
Li^+	1.508	125.8
Na^+	1.501	125.8
K^+	1.511	127.5
Mg^{2+}	1.473	120.4

effect of various cations (Li^+, Na^+, K^+, Mg^{2+} on the calculated $C_{NHC}-CO_2$ bond distances in H_2O. In each case there is a substantial reduction in the $C_{NHC}-CO_2$ bond distance relative to the uncomplexed **1** in the H_2O (1.522 Å) or the gas phase (1.576 Å). The most substantial decrease was with magnesium dication (1.473 Å).

The effect a cation would have on the decomposition rate of **1** was also probed. Our initial thinking was that the cation binding to the carboxylate moiety would decrease the rate of decarboxylation. The results are outlined in Table 7 as initial rates of decomposition were acquired in 1,4-dioxane/water solutions. We used higher water concentrations to allow for increased concentrations of the added chloride salts. Again, we observe a similar trend as witnessed in Table 1, that is, with increasing water concentrations the slower the rate of decomposition. However, we did observe a decrease in the rate with added salts versus no addition of salts at 20% water in 1,4-dioxane. Though the size of the cation (Li^+, Na^+, K^+) did not have much of an effect on the rate of decomposition, we did observe around a 22% decrease in the rate with lithium chloride as opposed to no salt. An even greater effect could be seen with the more electropositive magnesium cation as a 39% decrease in the rate of decomposition was observed.

■ CONCLUSIONS

The experimental kinetic studies along with DFT calculations show that solvent polarity has a dramatic effect on the stability of

dx.doi.org/10.1021/jo5007575 | J. Org. Chem. 2014, 79, 4293−4299

Table 7. Decomposition Rate Constants of 1 in 1,4-Dioxane/H_2O Mixtures with Chloride Salts[a]

% H_2O	Li^+	Na^+	K^+	Mg^{2+}
20.0	$(2.01 \pm 0.09) \times 10^{-4}$	$(2.04 \pm 0.15) \times 10^{-4}$	$(2.00 \pm 0.04) \times 10^{-4}$	$(1.59 \pm 0.06) \times 10^{-4}$
25.0	$(9.26 \pm 0.76) \times 10^{-5}$	$(9.49 \pm 0.38) \times 10^{-5}$	$(8.66 \pm 0.32) \times 10^{-5}$	$(8.00 \pm 0.43) \times 10^{-5}$
30.0	$(4.60 \pm 0.28) \times 10^{-5}$	$(4.85 \pm 0.73) \times 10^{-5}$	$(4.51 \pm 0.37) \times 10^{-5}$	$(3.67 \pm 0.26) \times 10^{-5}$

[a][LiCl] = 40.0 mM, [NaCl] = 40.4 mM, [KCl] = 39.8 mM, [$MgCl_2$] = 39.9 mM.

NHC−CO_2 complexes. For example, the Gibbs free energy for binding of CO_2 to carbene **3** ranges from ca. 4 kcal/mol in the gas phase to 24 kcal/mol in water. As seen in the simple valence bond representation, bond formation between NHCs and CO_2 is accompanied by charge transfer from the carbene to the carboxylate substituent. Polar solvents favor shorter and stronger C_{NHC}−CO_2 bonds, whereas nonpolar solvents favor longer and weaker C_{NHC}−CO_2 bonds. The ability to optimize CO_2 binding energies either through solvent, as shown in this study, and/or substituents, as shown in previous work, can be applied to the development of CO_2 reduction catalysts.

EXPERIMENTAL SECTION

Kinetic Studies. Decomposition initial rate constants of **1** were measured by monitoring the decrease in absorbance at 240 nm over time by UV−vis in a 1 cm quartz cuvette capped with a septum that was oven-dried prior to use. HPLC-grade water, methanol, and acetonitrile were used. The acetonitrile was distilled over CaH_2 and stored with 4 Å molecular sieves. Spectrophotometric grade 1,4-dioxane was used to minimize any absorbance overlap at 240 nm. The concentration of **1** in the kinetic studies ranged ca. 0.2−0.4 mM. Initial rate constants of decomposition are expressed in s^{-1}, and the average of 3 runs was used to determine the reported rate constant.

DFT Calculations. Calculations were done using Gaussian 09[37] with the basis set B3LYP/6-31G(d,p)[27,28] and the SMD implicit solvation model.[29] Ground-state geometries of **1** listed in Table 5 represent optimized minima. Transition-state geometries were optimized by QST3 following a scan calculation of the C_{NHC}−CO_2 bond (30−40 scans in 0.05 Å increments). The free energy of activation was also calculated for **1** in water for three other implicit solvation models.

Experimental Free Energy of Activation. An Eyring plot was used to experimentally determine the free energy of activation to decarboxylation of **1** in water using a temperature-controlled cuvette holder and monitoring the decrease in absorbance at 240 nm over time. A similar concentration range was used to that of the aforementioned kinetic studies and the average of three runs were used to determine the rate constant at 353, 358, 363, 368 K.

Synthesis of 1,3-Dimethylimidazolium-2-Carboxylate (1). To a 30 mL screw top pressure tube were added 1-methylimidazole (4.00 mL, 50.2 mmol) and dimethyl carbonate (6.00 mL, 71.2 mmol). The tube was sealed and allowed to stir in an oil bath behind a blast shield for 48 h at a temperature of 95 ± 5 °C. After the allotted time, the reaction was allowed to cool to room temperature and the screw cap was removed. The liquid was decanted off and the remaining white crystals were allowed to stir in diethyl ether for 30 min. The crystals were vacuum filtered and rinsed with generous portions of diethyl ether, acetone, and acetonitrile. The remaining white crystals were transferred to a preweighed vial and allowed to dry under vacuum (2.14 g, 30.4%). Reported characterization data are consistent with previously reported results:[25] ^{1}H NMR (400 MHz, D_2O) δ 7.37 (s, 2H), 3.99 (s, 6H); ^{13}C NMR (400 MHz, D_2O), δ 158.71, 140.16, 123.45, 37.14. FT-IR 1642 cm^{-1}.

ASSOCIATED CONTENT

Supporting Information

Decomposition plots for the reported initial rate constants (Tables 1−3 and 7) and calculated geometries and energies under different implicit solvation models (Tables 4−6). The material is available free of charge via the Internet at http://pubs.acs.org.

AUTHOR INFORMATION

Corresponding Author

*E-mail: falvey@umd.edu.

Notes

The authors declare no competing financial interest.

ACKNOWLEDGMENTS

This work was supported by the American Chemical Society Petroleum Research Foundation.

REFERENCES

(1) Stauffer, P. H.; Keating, G. N.; Middleton, R. S.; Viswanathan, H. S.; Berchtold, K. A.; Singh, R. P.; Pawar, R. J.; Mancino, A. *Environ. Sci. Technol.* **2011**, *45*, 8597−8604.
(2) Markewitz, P.; Kuckshinrichs, W.; Leitner, W.; Linssen, J.; Zapp, P.; Bongartz, R.; Schreiber, A.; Müller, T. E. *Energy Environ. Sci.* **2012**, *5*, 7281−7305.
(3) Appel, A. M.; et al. *Chem. Rev.* **2013**, *113*, 6621−6658.
(4) Sumida, K.; Rogow, D. L.; Mason, J. A.; McDonald, T. M.; Bloch, E. D.; Herm, Z. R.; Bae, T.-H.; Long, J. R. *Chem. Rev.* **2012**, *112*, 724−728.
(5) Goeppert, A.; Czaun, M.; May, R. B.; Prakash, G. K. S.; Olah, G.; Narayanan, S. R. *J. Am. Chem. Soc.* **2011**, *133*, 20164−20167.
(6) Lu, W.; Sculley, J. P.; Yuan, D.; Krishna, R.; Wei, Z.; Zhou, H.-C. *Angew. Chem., Int. Ed.* **2012**, *51*, 7480−7484.
(7) Ashley, A. E.; Thompson, A. L.; O'Hare, D. *Angew. Chem., Int. Ed.* **2009**, *48*, 9839−9843.
(8) Mömming, C. M.; Otten, E.; Kehr, G.; Fröhlick, R.; Grimme, S.; Stephan, D. W.; Erker, G. *Angew. Chem., Int. Ed.* **2009**, *48*, 6643−6646.
(9) Ménard, G.; Stephan, D. W. *J. Am. Chem. Soc.* **2010**, *132*, 1796−1797.
(10) Jutz, F.; Andanson, J.-M.; Baiker, A. *Chem. Rev.* **2011**, *111*, 322−353.
(11) Kuhn, N.; Niquet, E.; Steimann, M.; Walker, I. *Z. Naturforsch., B* **1999**, *54*, 427−433.
(12) Kayaki, Y.; Yamamoto, M.; Ikariya, T. *Angew. Chem., Int. Ed.* **2009**, *48*, 4194 −4197.
(13) Zhou, H.; Zhang, W.; Liu, C.; Qu, J.; Lu, Z. *J. Org. Chem.* **2008**, *73*, 8039−8044.
(14) Voutchkova, A. M.; Appelhans, L. H.; Chianese, A. R.; Crabtree, R. H. *J. Am. Chem. Soc.* **2005**, *127*, 17624−17625.
(15) Voutchkova, A. M.; Feliz, M.; Clot, E.; Eisenstein, O.; Crabtree, R. H. *J. Am. Chem. Soc.* **2007**, *129*, 12834−12846.
(16) Tudose, A.; Demonceau, A.; Delaude, L. *J. Organomet. Chem.* **2006**, *691*, 5356−5365.
(17) Kayaki, Y.; Yamamoto, M.; Ikariya, T. *Angew. Chem.* **2009**, *121*, 4258−4261.
(18) Tommasi, I.; Sorrentino, F. *Tetrahedron Lett.* **2005**, *46*, 2141−2145.
(19) Tommasi, I.; Sorrentino, F. *Tetrahedron Lett.* **2009**, *50*, 104−107.
(20) Hans, M.; Delaude, L.; Rodriguez, J.; Coquerel, Y. *J. Org. Chem.* **2014**, *79*, 2758−2764.
(21) Fèvre, M.; Pinaud, J.; Leteneur, A.; Gnanou, Y.; Vignolle, J.; Taton, D. *J. Am. Chem. Soc.* **2012**, *134*, 6776−6784.
(22) Fèvre, M.; Coupillaud, P.; Miqueu, K.; Sotiropoulous, J.-M.; Vignolle, J.; Taton, D. *J. Org. Chem.* **2012**, *77*, 10135−10144.

(23) Ajitha, M. J.; Suresh, C. H. *J. Org. Chem.* **2012**, *77*, 1087−1094.
(24) Van Ausdall, B. R.; Poth, N. F.; Kincaid, V. A.; Arif, A. M.; Louie, J. *J. Org. Chem.* **2011**, *76*, 8413−8420.
(25) Holbrey, J. D.; Reichert, W. M.; Tkatchenko, I.; Bouajila, E.; Walter, O.; Tommasi, I.; Rogers, R. D. *Chem. Commun.* **2003**, 28−29.
(26) Amyes, T. L.; Diver, S. T.; Richard, J. P.; Rivas, F. M.; Toth, K. *J. Am. Chem. Soc.* **2004**, *126*, 4366−4374.
(27) Becke, A. D. *J. Phys. Chem.* **1993**, *98*, 1372−1377.
(28) Lee, C.; Yang, W.; Parr, R. G. *Phys. Rev. B* **1988**, *37*, 785−789.
(29) Marenich, A. V.; Cramer, C. J.; Truhlar, D. G. *J. Phys. Chem. B* **2009**, *113*, 6378−6396.
(30) Klamt, A.; Schüürmann, G. *J. Chem. Soc., Perkin Trans. 2* **1993**, 799−805.
(31) Andzelm, J.; Kölmel, C.; Klamt, A. *J. Chem. Phys.* **1995**, *103*, 9312−9320.
(32) Cancès, E.; Mennucci, B.; Tomasi, J. *J. Chem. Phys.* **1997**, *8*, 3032−3042.
(33) Miertus, S.; Scrocco, E.; Tomasi, J. *Chem. Phys.* **1981**, *55*, 117−129.
(34) Barone, V.; Cammi, R.; Tomasi, J. *Chem. Phys. Lett.* **1996**, *255*, 327−335.
(35) Dimroth, K.; Reichardt, C.; Siepmann, T.; Bohlmann, F. *Liebigs Ann. Chem.* **1963**, *661*, 1−37.
(36) Reichardt, C. *Liebigs Ann. Chem.* **1971**, *752*, 64−67.
(37) Gaussian 09, Revision D.01, Frisch, M. J.; Trucks, G. W.; Schlegel, H. B.; Scuseria, G. E.; Robb, M. A.; Cheeseman, J. R.; Scalmani, G.; Barone, V.; Mennucci, B.; Petersson, G. A.; Nakatsuji, H.; Caricato, M.; Li, X.; Hratchian, H. P.; Izmaylov, A. F.; Bloino, J.; Zheng, G.; Sonnenberg, J. L.; Hada, M.; Ehara, M.; Toyota, K.; Fukuda, R.; Hasegawa, J.; Ishida, M.; Nakajima, T.; Honda, Y.; Kitao, O.; Nakai, H.; Vreven, T.; Montgomery, J. A., Jr.; Peralta, J. E.; Ogliaro, F.; Bearpark, M.; Heyd, J. J.; Brothers, E.; Kudin, K. N.; Staroverov, V. N.; Kobayashi, R.; Normand, J.; Raghavachari, K.; Rendell, A.; Burant, J. C.; Iyengar, S. S.; Tomasi, J.; Cossi, M.; Rega, N.; Millam, N. J.; Klene, M.; Knox, J. E.; Cross, J. B.; Bakken, V.; Adamo, C.; Jaramillo, J.; Gomperts, R.; Stratmann, R. E.; Yazyev, O.; Austin, A. J.; Cammi, R.; Pomelli, C.; Ochterski, J. W.; Martin, R. L.; Morokuma, K.; Zakrzewski, V. G.; Voth, G. A.; Salvador, P.; Dannenberg, J. J.; Dapprich, S.; Daniels, A. D.; Farkas, Ö.; Foresman, J. B.; Ortiz, J. V.; Cioslowski, J.; Fox, D. J. Gaussian, Inc., Wallingford, CT, 2009.

dx.doi.org/10.1021/jo5007575 | *J. Org. Chem.* 2014, 79, 4293−4299